AAS 21-602

CARTESIAN RELATIVE MOTION ON PERTURBED ECCENTRIC ORBITS AND CLOSED-FORM SOLUTION FOR J2 EFFECTS AT LOW INCLINATIONS

Matthew Willis* **and Simone D'Amico†**

Two contributions to the study of perturbed relative motion in the radial-transverse-normal frame of an eccentric orbit are introduced. First, a general form of the governing equations is developed, allowing for any perturbation and choice of independent variable. Next, these are simplified and solved for the practical case of equatorial orbits subject to Earth oblateness perturbation. This results in a novel analytical solution that is shown to be orders of magnitude more accurate than other translational state models in the literature. The new solution is evaluated across a wide range of eccentricities and inclinations, and is applicable to hyperbolic trajectories as well as elliptical orbits.

INTRODUCTION

The development of precise analytical models for the motion of celestial bodies is among the oldest pursuits of mathematical physics. In the four centuries since Kepler first described how the planets proceed on their elliptical trajectories, more sensitive measurements and more demanding applications have prompted ever more accurate models of orbital motion. These advances are driven today by the guidance and navigation requirements of man-made spacecraft, whether exploring the solar system or performing essential tasks in Earth orbit. Distributed space systems are of great interest in both domains as an enabling technology for applications ranging from inspection and servicing of Earth-orbiting satellites to interior studies of small bodies in the solar system, observations of gravitational waves, and direct imaging of extrasolar planets. Although modern understanding of the forces that act on a spacecraft provides equations of relative motion that can be numerically integrated with very high accuracy, analytical solutions are more valuable than ever for trajectory design, maneuver planning, and orbit determination tasks that require inversion of the dynamics, and when the limited processing power typical of spaceflight hardware makes numerical integration impractical. This work advances the state of the art in analytical modeling of spacecraft dynamics with the introduction of a solution for relative position and velocity with respect to an eccentric orbit near the equatorial plane of an oblate body.

Relative dynamics models are broadly divided between those based on orbital elements, which capture the underlying physical and geometric properties of the motion, and those using a translational state representation, which closely relates to the system observables.[1] The present work builds upon the body of literature concerned with solving the differential equations that govern the position vector of a deputy spacecraft relative to a chief in a frame rotating with the latter's orbital motion.

*PhD Candidate, Department of Aeronautics and Astronautics, Stanford University, 496 Lomita Mall, Stanford, CA 94305.
†Professor, Department of Aeronautics and Astronautics, Stanford University, 496 Lomita Mall, Stanford, CA 94305.

This corpus includes the well-known Clohessy-Wiltshire (CW) solution, which addresses the linear, time-invariant problem of close proximity relative motion on near-circular orbits.[2] Yamanaka and Ankersen (YA) generalized CW to eccentric orbits with a solution of the linear, time-varying Tschauner-Hempel (TH) equations.[3,4] Other authors have built upon the foundation of YA and CW to develop more accurate models by incorporating higher-order effects from spherical gravity, as well as the effects of non-Keplerian perturbations. London and Sasaki used the method of successive approximations to develop a second-order solution to the circular-orbit problem.[5,6] Willis, Lovell, and D'Amico (WLD) applied a similar technique to extend YA into a second-order eccentric orbit solution.[7] Each of these extensions assumes that the only force acting on the spacecraft is due to the central body's point-mass gravity field.

In reality, space missions are perturbed by interactions with the atmosphere and other celestial bodies, as well as the gravitational effects of Earth's nonspherical mass distribution. For missions below GEO, the most persistent and significant of these perturbations is the effect of Earth's oblateness, captured by the J_2 coefficient in the spherical harmonic representation of the gravitational field.[8] Much recent work in the relative dynamics literature has sought to incorporate the effects of this perturbation in analytical models. Schweighart and Sedwick used averaging techniques to describe the relative dynamics on near-circular orbits subject to J_2 perturbation as a time-invariant system.[9] Butcher and Burnett developed a solution to the time-varying dynamics on J_2-perturbed, circular orbits without averaging.[10] Ogundele and Agboola also built upon their power series solutions to the TH equations with a model incorporating J_2 effects.[11,12] The authors of the present paper recently introduced a partial solution for J_2 corrections to their second-order solution for relative position and velocity.[13] In addition to differences in their assumptions on the dynamics, these models are distinguished by their choices of independent variable. The time-invariance of the circular orbit problem allows for the use of time as the independent variable in the CW solution and its higher order extension by London, Sasaki, and others. Butcher and Burnett built upon the earlier work of Melton to develop time-explicit approximations of the effect of eccentricity on near-circular orbits, and similarly used time as the independent variable in their J_2 solution.[14,15] Models for more general eccentric orbits based on the TH equations typically use true anomaly as the independent variable. This includes YA, its higher-order extension WLD, as well as Ogundele and Agboola's power series solutions. However, true anomaly is a poor variable for characterizing perturbed motion and the authors elected to use the argument of latitude as the fast variable in their previous J_2 solution development.

The body of this paper is divided into three parts. The first begins by unifying the relative dynamics literature with the introduction of a general set of equations governing the relative position and velocity for any choice of independent variable and subject to any prescribed perturbation. A general methodology for developing analytical solutions by a combination of successive approximations and variation of parameters is then described. The middle part simplifies the general equations for the special case of J_2 perturbation on eccentric, equatorial orbits and introduces an analytical solution for the leading-order corrections. Because argument of latitude is undefined for equatorial orbits, the true longitude is used as independent variable in these developments. The third part evaluates the accuracy of the new solution and compares it with several of the models discussed in this section. The evaluation spans a range of eccentricities and low-inclination orbits, and includes an examination of the new solution's applicability to hyperbolic trajectories. The paper concludes with a summary of contributions and potential avenues for future research.

GENERAL PERTURBATION FRAMEWORK

Equations of Relative Motion

Before narrowing focus to Earth oblateness perturbation and near-equatorial orbits, we will consider the relative motion dynamics when general perturbing accelerations $\mathbf{d}$ and $\mathbf{d}_d$ are experienced by the chief and deputy, respectively. This section fills a gap in the existing literature by building up the equations of relative motion in the chief's orbital frame in a form suitable for application to general perturbations, any choice of independent variable, and arbitrary accuracy. Let $\mathbf{r}$ represent the position vector from the central body to the chief spacecraft and $\mathbf{r}$ be the relative position vector of the deputy with respect to the chief. According to the fundamental orbital differential equation, the relative dynamics in the inertial frame I are governed by

$$^{I}\mathbf{r} = \mu\left(\frac{\mathbf{r} + \mathbf{r}}{k\mathbf{r} + \mathbf{r}k^3} - \frac{\mathbf{r}}{r^3}\right) + \mathbf{d}_d - \mathbf{d} \tag{1}$$

where $^{I}(\_)$ indicates a time derivative with respect to an inertial frame, μ is the gravity parameter of the central body, and $r = k\mathbf{r}k$ is the chief's orbit radius. Let L denote the Hill frame which rotates with the chief's motion around the central body at the orbital angular velocity $\boldsymbol{\omega}$.[16] The theorem of Coriolis relates the relative motion with respect to L to the motion in I according to

$$^{L}\mathbf{r} = {}^{I}\mathbf{r} - 2\boldsymbol{\omega} \quad \mathbf{v} - \underline{\boldsymbol{\omega}} \quad \mathbf{r} - \boldsymbol{\omega} \quad \boldsymbol{\omega} \quad \mathbf{r} \tag{2}$$

where $\mathbf{v} \quad {}^{L}\underline{\mathbf{r}}$ is the relative velocity with respect to L. Equations (1) and (2) give an exact, coordinate-independent description of the relative motion with respect to the Hill frame. However, their utility for the development of analytical solutions is limited by the use of time as the independent variable.

Tschauner and Hempel demonstrated that an elegant form of the equations of relative motion suitable for unperturbed eccentric orbits can be obtained through normalization of the coordinates by the orbit radius r and use of true anomaly f as independent variable. Letting $(\tilde{\ })$ denote the normalized coordinates and $()'$ be derivatives with respect to the new independent variable, these transformations are given by

$$\begin{aligned} \tilde{\mathbf{r}} &= \frac{1}{r}\,\mathbf{r} \\ \tilde{\mathbf{v}} &= \frac{e}{p}\,\mathbf{r}\sin f + \frac{1}{k}\sqrt{\frac{p}{\mu}}\,\mathbf{v} \end{aligned} \tag{3}$$

$$\begin{aligned} \mathbf{r} &= r\,\tilde{\mathbf{r}} \\ \mathbf{v} &= \sqrt{\frac{\mu}{p}}\,(e\,\tilde{\mathbf{r}}\sin f + k\,\tilde{\mathbf{v}}) \end{aligned} \tag{4}$$

where $\tilde{\mathbf{v}} \quad {}^{L}\tilde{\mathbf{r}}'$, $p = a(1 \quad e^2)$ is the semi-latus rectum, and

$$k = \frac{p}{r} = 1 + e\cos f \tag{5}$$

The relative position vector is frequently expressed in radial-transverse-normal (RTN) coordinates, often called the local-vertical local-horizontal coordinates, attached to the chief's Hill frame L as $\tilde{\mathbf{r}} = [x, y, z]^T$. The RTN coordinates are defined with the chief at the origin, the x-axis directed radially away from the central body, the z-axis parallel to the chief's orbital angular momentum

vector $\mathbf{r}$ $\mathbf{v}$, and the y-axis completing the right-handed triad. To avoid confusion with other orientations of x, y, and z in the literature, the corresponding components of vectors other than relative position and velocity will be designated with subscripts R, T, and N.

The advantage of true anomaly as independent variable stems from the fact that for unperturbed orbits $f = \omega_N$ and $\omega_R = \omega_T = 0$. This greatly simplifies the expression of the fictitious forces in Equation (2). The effect of perturbations on the argument of perigee ω (not to be confused with the angular velocity and its components), right ascension of the ascending node , and inclination i disrupt the simple relationship between true anomaly and angular velocity. For a perturbation $\mathbf{d} = [d_R, d_T, d_N]^T$ acting on the chief, the true anomaly rate is given by

$$f = \frac{n}{\eta^3}k^2 + \frac{\eta}{nae}\left[d_R \cos f \quad d_T\left(1 + \frac{1}{k}\right)\sin f\right] \tag{6}$$

where $\eta = \sqrt{1 \quad e^2}$ and $n = \sqrt{\mu/a^3}$ is the mean motion.[17] For near-circular orbits, perturbations can have a significant effect on the ill-defined true anomaly, making it a poor choice of independent variable. In previous work on relative motion of J_2-perturbed eccentric orbits, the authors showed that the argument of latitude $u = \omega + f$ is a more practical choice for inclined orbits. Whereas true anomaly is directly affected by in-plane perturbations, only the out-of-plane perturbation appears in the equation governing the argument of latitude rate,

$$\underline{u} = \frac{n}{\eta^3}k^2 \quad \frac{\eta}{na}\frac{\cos i}{\sin i}\frac{\sin u}{k}d_N \tag{7}$$

For near-equatorial orbits, it will be preferable to use the quantity $u + \cos i$ because in general

$$\omega_N = \underline{u} + \_ \cos i = \frac{n}{\eta^3}k^2 \tag{8}$$

The choice of independent variable may depend on the specific problem being addressed, so this discussion will adopt the generic angular variable α.

Perturbations affect the relative dynamics in the transformed RTN coordinates in several ways. The most immediately apparent is the differential inertial acceleration $\mathbf{d}_d$ $\mathbf{d}$ appearing in Equation (1). Slightly more subtle is the variation in the chief's orbital angular velocity ! in Equation (2). In the presence of perturbations, the chief's angular velocity and acceleration expressed in RTN components are

$$! = \begin{bmatrix} \frac{d_N}{r\omega_N} \\ 0 \\ \omega_N \end{bmatrix} \qquad \underline{!} = \begin{bmatrix} \frac{d_{c,N}}{r\omega_N} + \frac{r}{r^2}\frac{d_N}{\omega_N} & \frac{d_T d_N}{r^2\omega_N^2} \\ 0 \\ \frac{d_T}{r} \quad 2\omega_N\frac{r}{r} \end{bmatrix} \tag{9}$$

where $\frac{r}{r} = \frac{\omega_N}{k}e\sin f$. As in Equation (8), ω_N is the component of angular velocity in the direction normal to the orbit plane defined by the chief's position and velocity vectors. The orbital angular velocity and angular momentum vectors are parallel for Keplerian motion, but out-of-plane perturbations create a rotational moment which appears explicitly in the angular velocity vector and causes the angular momentum vector to vary over time. The normal component of $\underline{!}$ in Equation (9) shows how along-track perturbations affect ω_N. These subtleties are commonly neglected in the literature.

The effects of differential inertial acceleration and of perturbations on the chief's orbital motion are fundamental to the relative dynamics in the RTN frame and independent of the transformations of Equations (3) and (4). Because perturbations affect the chief's orbit radius and progress in its orbit, the coordinate normalization and change of independent variable will introduce additional effects that must be accounted for. Applying Leibniz's rule to $\mathbf{r}$ in Equation (4), we find

$$\begin{aligned} \underline{\mathbf{r}} &= r\,\hat{\mathbf{r}} + \underline{r}\,\mathbf{r} \\ \ddot{\mathbf{r}} &= r\,\hat{\mathbf{r}} + 2\underline{r}\,\hat{\mathbf{r}} + \ddot{r}\,\mathbf{r} \end{aligned} \tag{10}$$

where

$$\ddot{r} = r\omega_N^2\left(1 - \frac{1}{k}\right) + d_R \tag{11}$$

and it is implied that the vector derivatives are taken with respect to L. For a general quantity x, the chain rule allows us to recast time derivatives in terms of the new independent variable according to $\underline{x} = \frac{dx}{dt} = \frac{dx}{d\alpha}\frac{d\alpha}{dt} = \underline{\alpha}x'$. We may therefore write

$$\begin{aligned} \underline{\mathbf{r}} &= \underline{\alpha}\,\mathbf{r}' \\ \ddot{\mathbf{r}} &= \underline{\alpha}\left(\underline{\alpha}\,\mathbf{r}'\right)' = \underline{\alpha}^2\,\mathbf{r}'' + \underline{\alpha}'\,\mathbf{r}' \end{aligned} \tag{12}$$

The second line invokes the fact that $\underline{\alpha}\underline{\alpha}' = \frac{d\alpha}{dt}\frac{d}{d\alpha}\left(\frac{d\alpha}{dt}\right) = \frac{d^2\alpha}{dt^2} = \underline{\alpha}'$.

The combination of Equations (1)-(5) and (9)-(12) constitute an exact description of the perturbed relative motion in the RTN frame of the chief spacecraft in normalized coordinates and with arbitrary choice of independent variable α. Before putting these pieces together into a single expression for $\mathbf{r}''$, it will be instructive to expand the differential Keplerian gravity and take advantage of cancellations that occur in the derivation of the Tschauner-Hempel equations. In particular, the binomial series expansion can be used to rewrite the point-mass gravity terms of Equation (1) as

$$\begin{aligned} \mu\left(\frac{\mathbf{r}+\boldsymbol{\rho}}{k\|\mathbf{r}+\boldsymbol{\rho}\|^3} - \frac{\mathbf{r}}{r^3}\right) &= \frac{\mu}{r^2}\left(\frac{(\hat{\mathbf{r}}+\boldsymbol{\rho})}{(1+\chi)^{3/2}} - \hat{\mathbf{r}}\right) \\ &= \frac{r\omega_N^2}{k}\left[\boldsymbol{\rho} + (\hat{\mathbf{r}}+\boldsymbol{\rho})\sum_{m=1}^{1}\frac{(-1)^m}{m!}\chi^m\prod_{j=0}^{m}\left(\frac{3}{2}+j\right)\right] \end{aligned} \tag{13}$$

where $\hat{\mathbf{r}}$ denotes a unit vector in the radial direction and

$$\chi^m = \sum_{l=0}^{m}\binom{m}{l}(2x)^{m-l}(\boldsymbol{\rho}^T\boldsymbol{\rho})^l \tag{14}$$

Equations (13) and (14) can be used to express the effects of differential Keplerian gravity to arbitrary precision. For example, including terms up to third order in the relative state variables gives

$$\mu\left(\frac{\mathbf{r}+\boldsymbol{\rho}}{k\|\mathbf{r}+\boldsymbol{\rho}\|^3} - \frac{\mathbf{r}}{r^3}\right) \approx \frac{r\omega_N^2}{k}\left(\boldsymbol{\rho} + \begin{bmatrix}3x\\0\\0\end{bmatrix} + 3\begin{bmatrix}x^2 & \frac{1}{2}(y^2+z^2)\\ xy & \\ xz & \end{bmatrix} + \begin{bmatrix}4x^2+6xy^2+6xz^2 & & \\ 6x^2y & \frac{3}{2}y^3 & \frac{3}{2}yz^2 \\ 6x^2z & \frac{3}{2}y^2z & \frac{3}{2}z^3\end{bmatrix}\right) \tag{15}$$

The term $\frac{r\omega_N^2}{k}\boldsymbol{\rho}$ from the linear part of Equation (15) cancels a term arising from the state transformation in Equations (10) and (11). The higher-order effects of differential Keplerian gravity

are often neglected, so these will be separated from the linear effects and treated as an additional perturbing acceleration given by

$$(\mathbf{d}_d \quad \mathbf{d})^{kep} = \frac{r\omega_N^2}{k}\left[\frac{3}{2}(\mathbf{r}^T \mathbf{r})\hat{\mathbf{r}} + (\hat{\mathbf{r}} + \mathbf{r})\sum_{m=2}^{1}\frac{(1)^m}{m!}\chi^m\prod_{j=0}^{m}\left(\frac{3}{2}+j\right)\right] \tag{16}$$

Putting all of the pieces together in a single expression for the relative acceleration in the RTN frame leads to

$$\begin{aligned}\mathbf{r}'' = {} & \frac{\omega_N^2}{\alpha^2}\left(\frac{3}{k}\begin{bmatrix}x\\0\\0\end{bmatrix} \quad \begin{bmatrix}0\\0\\z\end{bmatrix}\right) + 2\frac{\omega_N}{\alpha}\begin{bmatrix}y'\\x'\\0\end{bmatrix} \quad \left(\frac{\alpha'}{\alpha^2} + 2\frac{\omega_N}{\alpha}\frac{e\sin f}{k}\right)\mathbf{r}' + \frac{1}{r\alpha^2}(\mathbf{d}_d \quad \mathbf{d}) \quad \frac{\omega_N^2}{\alpha^2}\left(\frac{d_R}{r\omega_N^2}\right)\mathbf{r} \\ & + \frac{\omega_N^2}{\alpha^2}\left(\frac{d_T}{r\omega_N^2}\right)\begin{bmatrix}y\\x\\0\end{bmatrix} + \frac{\omega_N}{\alpha}\left(\frac{d_N}{r\omega_N^2}\right)\left\{2\begin{bmatrix}0\\z'\\y'\end{bmatrix} \quad \frac{\omega_N}{\alpha}\begin{bmatrix}z\\0\\x\end{bmatrix} + \left(\frac{r'}{r} + \frac{d_N'}{d_N} \quad \frac{\omega_N'}{\omega_N}\right)\begin{bmatrix}0\\z\\y\end{bmatrix} + \frac{\omega_N}{\alpha}\left(\frac{d_N}{r\omega_N^2}\right)\begin{bmatrix}0\\y\\z\end{bmatrix}\right\}\end{aligned} \tag{17}$$

Equation (17) combines the effects of differential inertial acceleration, perturbation of the reference frame's rotation, coordinate normalization, and change of independent variable. It applies for any perturbing forces and in conjunction with Equation (16) can be used to describe the relative motion to arbitrary accuracy. Although it is cumbersome, it provides a firm foundation upon which to lay assumptions and simplify the dynamics for the problem of interest. For example, if the perturbation on the chief acts only in the orbit plane, then $d_N = 0$ and the term in curly brackets vanishes entirely. Similarly, if the fast variable can be chosen such that $\alpha = \omega_N$, the expression simplifies to

$$\begin{aligned}\mathbf{r}'' = {} & \frac{3}{k}\begin{bmatrix}x\\0\\0\end{bmatrix} \quad \begin{bmatrix}0\\0\\z\end{bmatrix} + 2\begin{bmatrix}y'\\x'\\0\end{bmatrix} + \frac{1}{r\alpha^2}(\mathbf{d}_d \quad \mathbf{d}) \quad \left(\frac{d_R}{r\omega_N^2}\right)\mathbf{r} \quad \left(\frac{d_T}{r\omega_N^2}\right)\begin{bmatrix}x'\\y'+y\\z'\end{bmatrix} \\ & + \left(\frac{d_N}{r\omega_N^2}\right)\left\{\begin{bmatrix}z\\2z'\\2y' \quad x\end{bmatrix} + \left(\frac{r'}{r} + \frac{d_N'}{d_N} \quad \frac{\omega_N'}{\omega_N}\right)\begin{bmatrix}0\\z\\y\end{bmatrix} + \left(\frac{d_N}{r\omega_N^2}\right)\begin{bmatrix}0\\y\\z\end{bmatrix}\right\}\end{aligned} \tag{18}$$

The next section will show how Equation (17) simplifies for the specific case of Earth oblateness perturbation in equatorial orbits, but first we will describe how analytical solutions to Equation (17) may be obtained by the method of successive approximations and variation of parameters.

Solution by Successive Approximations

In many situations of interest it will not be possible to find exact analytical solutions to the relative dynamics in Equation (17), but approximate solutions can be very useful for guidance, navigation, and control (GNC) applications. This section outlines a practical method for obtaining such solutions by treating the complications arising from perturbations and higher-order gravity terms as corrections to the leading-order dynamics. In effect, the relative motion is expanded into the series

$$\mathbf{r} = \mathbf{r}_1 + \mathbf{r}_2 + \mathbf{r}_3 + \tag{19}$$

where $\mathbf{r}_1$ is the first-order solution for unperturbed relative motion, $\mathbf{r}_2$ captures second-order effects of Keplerian gravity and leading-order perturbation effects, and so on.

After dropping the perturbations and using $\alpha \quad \omega_N$, Equation (17) reduces to the familiar TH equations that govern $\mathbf{r}_1$,

$$\begin{aligned} x_1'' \quad \frac{3}{k}x_1 \quad 2y_1' &= 0 \\ y_1'' + 2x_1' &= 0 \\ z_1'' + z_1 &= 0 \end{aligned} \tag{20}$$

The solution to this system introduced by Yamanaka and Ankersen can be recast in terms of the general independent variable α, yielding

$$\begin{bmatrix} x_1 \\ y_1 \\ z_1 \\ x_1' \\ y_1' \\ z_1' \end{bmatrix} = \begin{bmatrix} (1 + \frac{3}{2}kk'J) & k\sin\alpha & k\cos\alpha & 0 & 0 & 0 \\ \frac{3}{2}k^2J & (1+k)\cos\alpha & (1+k)\sin\alpha & 1 & 0 & 0 \\ 0 & 0 & 0 & 0 & \sin\alpha & \cos\alpha \\ \frac{3}{2}\left((k'^2 + k(1 \quad k))J + \frac{k'}{k}\right) & (k\sin\alpha)' & (k\cos\alpha)' & 0 & 0 & 0 \\ \frac{3}{2}(2kk'J + 1) & \sin\alpha + (k\cos\alpha)' & \cos\alpha \quad (k\sin\alpha)' & 0 & 0 & 0 \\ 0 & 0 & 0 & 0 & \cos\alpha & \sin\alpha \end{bmatrix} \begin{bmatrix} K_1 \\ K_2 \\ K_3 \\ K_4 \\ K_5 \\ K_6 \end{bmatrix} \tag{21}$$

where $\mathbf{K} = [K_1, K_2, K_3, K_4, K_5, K_6]^T$ is a vector of integration constants that characterize the relative state and J is defined as the integral

$$J \quad \int \frac{d\alpha}{k^2} = \sqrt{\frac{\mu}{p^3}} \quad t \tag{22}$$

The second equality in Equation (22) follows from conservation of angular momentum and provides a convenient way to compute J from elapsed time. To avoid the explicit dependence of k on true anomaly in Equation (5), it can be rewritten as

$$k = 1 + e_x\cos\alpha + e_y\sin\alpha \tag{23}$$

where $e_x = e\cos(\alpha_0 \quad f_0)$ and $e_y = e\sin(\alpha_0 \quad f_0)$. The derivatives appearing in Equation (21) therefore become $k' = \quad e_x\sin\alpha + e_y\cos\alpha$, $(k\sin\alpha)' = \cos\alpha + e_x\cos 2\alpha + e_y\sin 2\alpha$, and $(k\cos\alpha)' = \quad \sin\alpha \quad e_x\sin 2\alpha + e_y\cos 2\alpha$.

Equation (21) provides a foothold for developing the subsequent approximations. Let $\mathbf{g}(\mathbf{r}, \alpha)$ represent the leading-order dynamics neglected by $\mathbf{r}_1$. Then the first correction $\mathbf{r}_2$ is governed by the system obtained by adding $\mathbf{g}(\mathbf{r}_1, \alpha)$ to the right-hand side of the TH equations. For example, in the case of second-order Keplerian gravity (cf. Equation (15)) the correction $\mathbf{r}_2$ is governed by

$$\begin{aligned} x_2'' \quad \frac{3}{k}x_2 \quad 2y_2' &= g_x(\mathbf{r}_1, \alpha) = \quad \frac{3}{k}x_1^2 + \frac{3}{2k}(y_1^2 + z_1^2) \\ y_2'' + 2x_2' &= g_y(\mathbf{r}_1, \alpha) = \frac{3}{k}x_1y_1 \\ z_2'' + z_2 &= g_z(\mathbf{r}_1, \alpha) = \frac{3}{k}x_1z_1 \end{aligned} \tag{24}$$

Crucially, the first-order solution is a known function of α and $\mathbf{K}$. By substituting $\mathbf{r}_1$ into the nonlinear and perturbation terms, the equations of motion have been cast as a linear, inhomogeneous system for $\mathbf{r}_2$. This procedure also decouples the out-of-plane dynamics from the motion in the plane. Proceeding with the latter, the second line of Equation (24) can be integrated once and used to eliminate y' from the x equation, according to

$$\begin{aligned} y_2' &= \quad 2x_2 + \int g_y(\alpha)d\alpha + c_{y1} \\ x_2'' + \left(4 \quad \frac{3}{k}\right)x_2 &= g_x(\alpha) + 2\int g_y(\alpha)d\alpha + 2c_{y1} \end{aligned} \tag{25}$$

where the dependence of $\mathbf{g}$ on $\mathbf{r}$ has been omitted to emphasize that it is a function only of α and constant parameters.

The general solution to the second-order linear, inhomogeneous ordinary differential equation on the second line of Equation (25) is

$$x_2 = c_{x1}\psi_1 + c_{x2}\psi_2 + \psi_p \tag{26}$$

where c_{x1} and c_{x2} are constants, ψ_1 and ψ_2 are linearly independent solutions to the corresponding homogeneous equation

$$x_2'' + \left(4 \quad \frac{3}{k}\right) x_2 = 0 \tag{27}$$

and ψ_p is the particular solution for the given forcing function $g_{xy}(\alpha) = g_x(\alpha) + 2\int g_y(\alpha)d\alpha + 2c_{y1}$.[18] For this system, two suitable homogeneous solutions are

$$\begin{aligned} \psi_1 &= k\sin\alpha \quad 2e_y\left(1 + \frac{3}{2}kk^{\emptyset}J\right) \\ \psi_2 &= k\cos\alpha \quad 2e_x\left(1 + \frac{3}{2}kk^{\emptyset}J\right) \end{aligned} \tag{28}$$

and the particular solution can be found from the variation of parameters formula

$$\psi_p = \psi_1 \int \frac{\psi_2 g_{xy}(\alpha)}{1 \quad e^2} d\alpha \quad \psi_2 \int \frac{\psi_1 g_{xy}(\alpha)}{1 \quad e^2} d\alpha \tag{29}$$

Once x_2 is known, y_2 is found by integrating the first line of Equation (25) with appropriate boundary conditions.

The out-of-plane motion is handled by a similar procedure, with the familiar harmonic oscillator dynamics leading to

$$z_2 = c_{z1}\sin\alpha + c_{z2}\cos\alpha + \phi_p \tag{30}$$

where the particular solution is given by

$$\phi_p = \sin\alpha \int g_z(\alpha)\cos\alpha d\alpha \quad \cos\alpha \int g_z(\alpha)\sin\alpha d\alpha \tag{31}$$

Although Equations (29) and (31) reduce the problem of solving Equation (24) to integration, there is no guarantee that the integrals can be evaluated in terms of elementary functions. Previous work by the authors showed that closed-form solutions can be found for second-order Keplerian gravity in both Cartesian and spherical coordinates.[19] The next section will show that this is also the case for the leading-order effects of J_2 perturbation in low-inclination orbits.

J_2-PERTURBED EQUATORIAL ORBITS

The second zonal harmonic of Earth's gravity field, characterized by the J_2 coefficient, causes a spacecraft to experience the perturbing acceleration

$$\mathbf{d}^{J_2} = \frac{1}{2}J_2\frac{\mu R_E^2}{r^5}\left[6(\hat{\mathbf{Z}} \quad \mathbf{r})\hat{\mathbf{Z}} + \left(3 \quad 15\frac{(\hat{\mathbf{Z}} \quad \mathbf{r})^2}{r^2}\right)\mathbf{r}\right] \tag{32}$$

where R_E is the Earth's equatorial radius and $\hat{\mathbf{Z}}$ is a unit vector parallel to Earth's spin axis. Expressed in the spacecraft's RTN frame this acceleration becomes

$$\mathbf{d}^{J_2} = \frac{3}{2}J_2\frac{\mu R_E^2}{r^4}\begin{bmatrix} 1 \quad 3\sin^2 i\sin^2 u \\ 2\sin^2 i\sin u\cos u \\ 2\sin i\cos i\sin u \end{bmatrix} \tag{33}$$

Because the argument of latitude u appears explicitly in the expression, it was the natural choice of independent variable in the authors' past analytical exploration of J_2-perturbed relative motion. However, u is undefined for equatorial orbits, motivating a separate treatment of this special case. A new reference vector in the equatorial plane must take the place of the ascending node, from which argument of latitude is measured. Choosing the vernal equinox, typically used as the X-direction in Earth-centered inertial coordinates, results in the true longitude defined by $\lambda = u +$. Conveniently, Equation (8) shows that for equatorial orbits $\lambda = \omega_N$. It is also apparent from Equation (33) that if $i = 0$, the transverse and normal components of the perturbation vanish and the acceleration due to J_2 is purely in the radial direction, $d_R = \frac{3}{2} J_2 \frac{\mu R_E^2}{r^4}$.

Substituting $d_T = d_N = 0$ and $\alpha = \lambda = \omega_N$ in the general relative motion dynamics of Equation (17) leads to

$$\tilde{\mathbf{r}}'' = \frac{3}{k} \begin{bmatrix} x \\ 0 \\ 0 \end{bmatrix} \quad \begin{bmatrix} 0 \\ 0 \\ z \end{bmatrix} + 2 \begin{bmatrix} y' \\ x' \\ 0 \end{bmatrix} + \frac{1}{r\omega_N^2} (\mathbf{d}_d \quad \mathbf{d}) \quad \left(\frac{d_R}{r\omega_N^2} \right) \tilde{\mathbf{r}} \tag{34}$$

This example illustrates the ease with which the equations of relative motion can be simplified from the general form to a more convenient form for the problem of interest. The first few terms in Equation (34) are the first-order effects captured by the TH equations. The last two terms represent the effects of the perturbation which must be addressed by the correction $\mathbf{r}_2$ of Equation (19). Because the successive approximations procedure linearizes the correction dynamics, the leading-order effects of J_2 can be treated independent of other effects such as higher-order Keplerian gravity and the resulting solutions may be combined by superposition. Thus, the second-order Keplerian effects that have been addressed in previous work will be neglected from the derivation but included in the validation section that follows.

The two perturbing terms of Equation (34) represent distinct influences of J_2 on the relative motion. The first is the differential inertial acceleration resulting from the different forces experienced by the two spacecraft due to their spatial separation. Expanding Equation (32) for the deputy spacecraft in the chief's RTN frame, truncating at first-order in the relative state variables, and subtracting the chief's acceleration for equatorial orbits leads to

$$\mathbf{g}_I = \frac{1}{r\omega_N^2} (\mathbf{d}_d \quad \mathbf{d}) = \frac{3}{2} J_2 \left(\frac{R_E}{p} \right)^2 k \begin{bmatrix} 4x \\ y \\ 3z \end{bmatrix} \tag{35}$$

Because the J_2 in near-equatorial orbits is predominantly radial, it is unsurprising that the differential acceleration is most sensitive to separations in this direction. The spacecraft closer to the central body will experience a stronger attraction due to J_2, accelerating the separation. Conversely, any offset from the radial axis introduces a restoring component in the differential perturbation. This effect is stronger in the normal direction because the oblate mass distribution represented by J_2 biases the attraction toward the equatorial plane.

The second contribution of J_2 to Equation (34) comes from the coordinate normalization. A perturbation that causes an increase in the chief's orbit radius ($d_R > 0$) will effectively reduce the normalized separation. Substituting the expression for d_R above leads to

$$\mathbf{g}_r = \left(\frac{d_R}{r\omega_N^2} \right) \tilde{\mathbf{r}} = \frac{3}{2} J_2 \left(\frac{R_E}{p} \right)^2 k \begin{bmatrix} x \\ y \\ z \end{bmatrix} \tag{36}$$

Remarkably, combining the expressions for $\mathbf{g}_I$ and $\mathbf{g}_r$ completely cancels the effect of J_2 in the transverse direction.

In addition to the two effects that appear explicitly in Equation (34), there is a practical correction that arises from the successive approximations approach. As shown in Equation (23), k depends on the chief's orbit geometry through e_x and e_y, which experience small variations due to J_2. The resulting deviations in k only contribute to higher-order effects in the perturbation terms of Equation (34), but they will have a leading-order effect in the $\frac{3}{k}$ term of the linear dynamics. Let k be the value of k computed when treating e_x and e_y as constants. Then, to a first approximation,

$$\frac{1}{k} \quad \frac{1}{k} \quad \frac{k}{k^2} \tag{37}$$

where $k = k \quad k$. The first term on the right-hand side is what appears in the linear dynamics, while the second term represents the leading-order correction for J_2. Substituting this into the equations of motion, we have

$$\mathbf{g}_k = \quad 3\frac{k}{k^2}\begin{bmatrix} x \\ 0 \\ 0 \end{bmatrix} \tag{38}$$

k is related to the variations in e_x and e_y by

$$k = \quad e_x \cos\lambda + \quad e_y \sin\lambda \tag{39}$$

where

$$\begin{aligned} e_x &= \int e_x' d\lambda = \quad \frac{3}{2} J_2 \left(\frac{R_E}{p}\right)^2 \int k^2 \sin\lambda d\lambda \\ e_y &= \int e_y' d\lambda = \quad \frac{3}{2} J_2 \left(\frac{R_E}{p}\right)^2 \int k^2 \cos\lambda d\lambda \end{aligned} \tag{40}$$

The integrals are evaluated from the initial to the present difference between the osculating and reference values of e_x and e_y. Although not essential, the mean orbital elements described by the theory of Brouwer and Lyddane provide practical reference values for use in the computation of k. Using $k \quad k$, the integrals can be evaluated analytically and $\quad k$ becomes

$$\begin{aligned} k = \frac{3}{2} J_2 \left(\frac{R_E}{p}\right)^2 \Bigg[& \frac{1}{3} \quad e_0 \cos(\lambda \quad \varpi_0) \quad k'(\lambda \quad \lambda_0) + \frac{1}{3}\left(1 + 2e^2 + 3k \quad k^2\right) \\ & \frac{1}{3}\left(1 + 2e^2 + k_0 + k_0^2\right)\cos(\lambda \quad \lambda_0) + \frac{2}{3} k_0 (k \quad 1) \Bigg] \end{aligned} \tag{41}$$

where $\varpi_0 = \lambda_0 \quad f_0$ and

$$e_0 = e\sqrt{1 \quad e^2} + \frac{e}{1 + \frac{p}{1 \quad e^2}} + \left(1 + k_0 + k_0^2\right)\cos f_0 \tag{42}$$

Combining Equations (35), (36), and (38), and substituting into $\mathbf{g}(\ \mathbf{r}_1, \alpha)$ in Equation (24) reveals that the correction $\ \mathbf{r}_2$ for J_2 perturbation in equatorial orbits is governed by

$$\begin{bmatrix} x_2'' & \frac{3}{k} x_2 & 2y_2' \\ y_2'' + 2x_2' \\ z_2'' + z_2 \end{bmatrix} = \frac{3}{2} J_2 \left(\frac{R_E}{p}\right)^2 \left(k \begin{bmatrix} 5x_1 \\ 0 \\ 2z_1 \end{bmatrix} \quad 3\frac{\hat{k}}{k^2} \begin{bmatrix} x_1 \\ 0 \\ 0 \end{bmatrix} \right) \tag{43}$$

where $\hat{k} = k/\left(\frac{3}{2}J_2\left(\frac{R_E}{p}\right)^2\right)$. At this stage, the expressions for $\mathbf{r}_1$ from Equation (21) can be substituted into the right-hand side and solved by the variation of parameters method described in the previous section. Despite the apparent simplicity of the first term on the right-hand side of Equation (43) and the apparent complexity of k in the second term, a closed-form solution for $\mathbf{r}_2$ may only be obtained when both are taken into account. The resulting analytical expressions for the J_2 corrections x_2, y_2, and z_2 are provided in the appendix. In accordance with Equation (19), these must be added to the linear solution of Equation (21) and can be combined with corrections for other effects such as second-order Keplerian gravity.

Before the new solution can be evaluated, there is one final detail that must be addressed. Just as the variations in k led to corrections in the first-order dynamics, they must be taken into account in the integral J that was defined in Equation (22). Using the same approximation $k = k +$ k as before, the definition of J can be expanded to

$$J = \int \frac{d\lambda}{k^2} \quad \int \left(1 + 2\frac{k}{k}\right)\frac{d\lambda}{k^2} \tag{44}$$

The first term in parentheses matches the unperturbed case, while the second term can be evaluated using k from Equation (41). Because we are primarily concerned with the secular growth of J, the short-period oscillations are neglected and J is approximated by

$$J = \int \frac{d\lambda}{k^2} \quad \sqrt{\frac{\mu}{p^3}} \quad t + \frac{3}{2}J_2\left(\frac{R_E}{p}\right)^2\left(\sqrt{\frac{\mu}{a^3}}\frac{t}{1 \quad e^2} + \frac{\lambda \quad \lambda_0}{k^2}\right) \tag{45}$$

Whereas J was a function of only the elapsed time t for Keplerian orbits, the perturbation adds an explicit dependence on the change in true longitude. Equipped with this new expression for J, the analytical solution for J_2-perturbed relative motion on equatorial orbits can be evaluated against the true dynamics and other models in the literature.

VALIDATION

This section will demonstrate the accuracy of the new analytical solution with respect to both the approximate and exact dynamics being considered. To add context, other prominent models from the literature are included in the comparison. We will first ground the analysis in a specific example scenario, then broaden the scope to show the impact of orbit eccentricity and inclination on solution performance, and to consider its applicability to hyperbolic trajectories.

Example Scenario

The chosen scenario was designed to exhibit typical relative motion behavior in a familiar mission profile. The chief is in a near-circular, low-earth orbit with $e = 0.001$, perigee altitude of 750 km, and, in accordance with the problem assumptions, $i = 0$. The relative motion is defined by the integration constant vector $a\mathbf{K} = [0.1, 2, 2, 5, 2, \quad 2]^T$ km. The first element indicates a positive radial offset due to a difference in semimajor axis that will cause the deputy to drift backward in the along-track direction. The next two elements introduce motion within the chief's orbit plane due to a differences in the eccentricity vectors. The fourth introduces a 5-km offset in the along-track direction. Finally, the last two constants represent a relative inclination vector phased with the relative eccentricity to ensure separation in the radial-normal plane as the deputy spacecraft

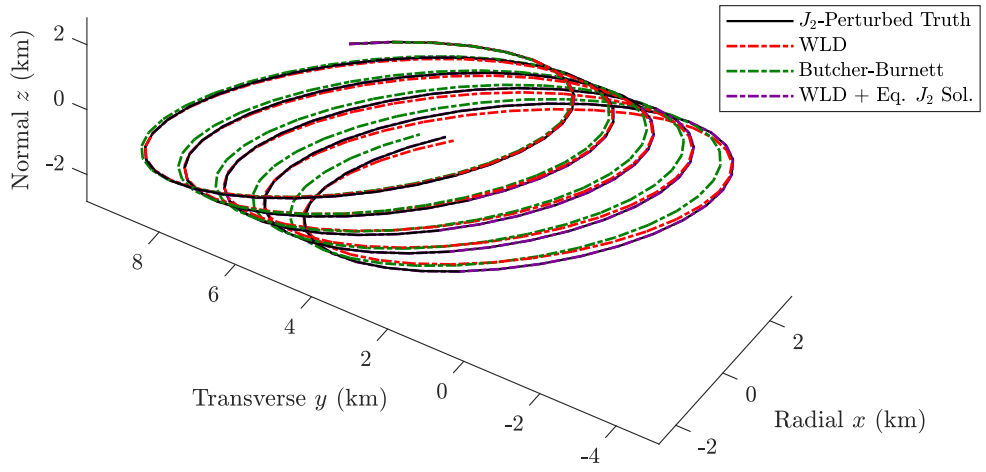

Figure 1. Relative Trajectory in the RTN Frame with $a\mathbf{K} = [0.1, 2, 2, 5, 2, \quad 2]^T$ km.

drifts toward the chief. All of these behaviors can be observed in Figure 1, which plots the relative trajectory in the RTN coordinate frame.

Four relative trajectory propagations are shown in Figure 1. First is the J_2-perturbed truth model, which is computed by numerically integrating the fundamental orbital differential equations for both chief and deputy using the perturbing acceleration defined in Equation (32), then taking their difference and rotating from inertial to RTN coordinates. Next is the Willis-Lovell-D'Amico (WLD) solution, which includes second-order Keplerian dynamics for eccentric orbits but neglects the effects of J_2. Shown in green is the Butcher-Burnett (BB) model, which includes J_2 and second-order Keplerian effects but assumes a circular orbit. Finally, the new J_2 corrections for equatorial orbits are combined with the second-order WLD solution in the purple curve. All three approximate models exhibit the general behavior described in the previous paragraph, but those that neglect the effects of orbit eccentricity or J_2 perturbation drift away from the truth model. In contrast, the new solution is indistinguishable from the true trajectory at the resolution of the figure.

While the plot in Figure 1 clearly illustrates the relative motion, the suppression of depth makes it difficult to assess how each model differs from the truth over time. To clarify these details, Figure 2 shows the propagation errors in each of the RTN coordinates as a function of the change in true longitude. In addition to the three relative motion models discussed above, it includes the Yamanaka-Ankersen (YA) solution, which neglects higher-order Keplerian effects along with J_2 perturbation. Both YA and BB exhibit secular error growth in the transverse direction due to failure to accurately capture the along-track drift. Errors in radial and normal directions tend to oscillate around the true motion, with amplitudes growing to hundreds of meters after a few orbits. The exception is the new solution, whose propagation errors are nearly indiscernible in the figure. These are shown more clearly in Figure 3, which replaces the less accurate models with two propagations closely related to the new analytical solution.

The black curve in Figure 3 is a numerical integration of the equations of relative motion including second-order Keplerian effects and leading-order J_2 effects. It may be viewed as a more

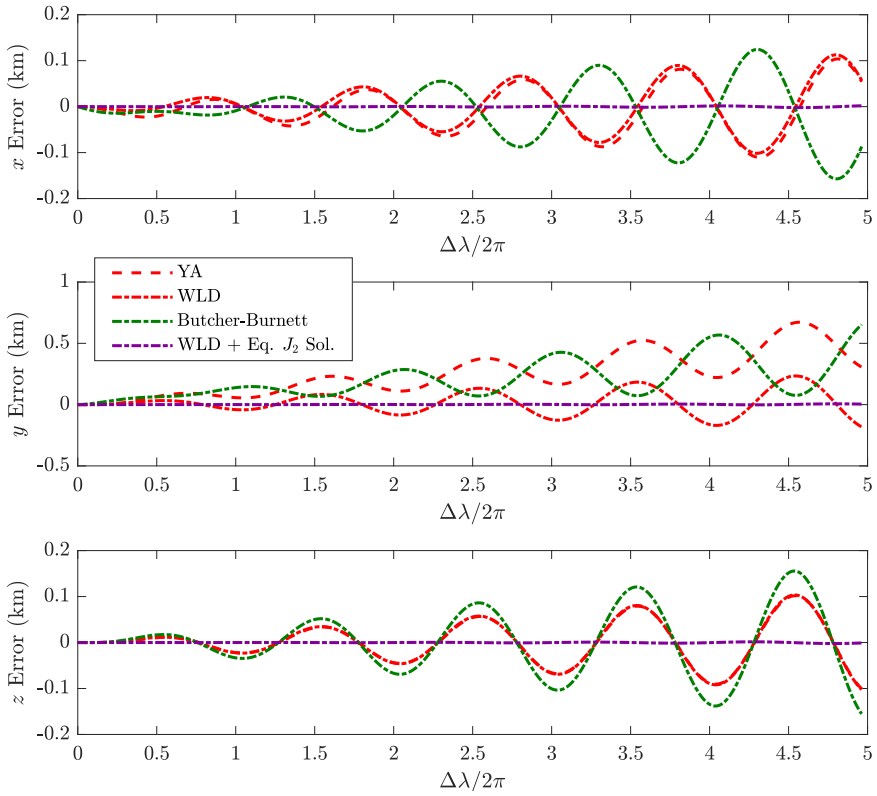

Figure 2. Error in Propagated RTN Components with $a\mathbf{K} = [0.1, 2, 2, 5, 2, \quad 2]^T$ km.

accurate version of the dynamics model in that it does not use the first-order solution to approximate the correction terms. The light purple line is the result of numerical integration when this additional step is included. It is therefore a numerical simulation of the analytical solution and the close agreement between the two demonstrates that the solution is correct. They differ only in the approximation of J from Equation (45) that is used to evaluate the analytical solution. Although the numerical integration of the less-approximate dynamics has smaller errors in x and z than the analytical solution, its error in y has a more pronounced secular growth. As a result, it has comparable overall error on the order of a meter per orbit.

Effect of Eccentricity

A major factor distinguishing the new solution for J_2-perturbed relative motion from those developed by Schweighart and Sedwick or Butcher and Burnett is its inclusion of eccentricity effects. This feature was not stressed by the circular-orbit test case considered above. The impact of eccentricity on solution accuracy can be observed by fixing the absolute and relative state initializations from the previous scenario while varying the orbit eccentricity at a constant perigee altitude of 750 km. The results are shown in Figure 4, with the mean eccentricity on the horizontal axis computed using the theory of Brouwer and Lyddane. To account for the scaling of the relative motion with orbit size as the eccentricity increases, the vertical axis shows the magnitude of the position error vector normalized by the inter-spacecraft separation. Furthermore, the error shown on the vertical axis is averaged over the fifth propagated orbit to provide a representative assessment of the solution accuracy.

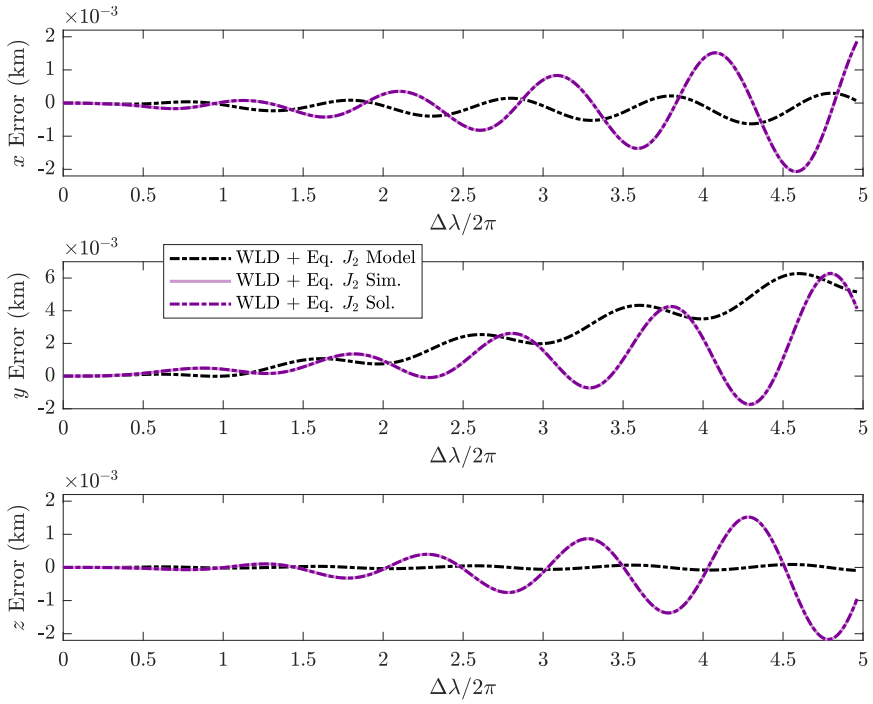

Figure 3. Error in Propagated RTN Components with $a\mathbf{K} = [0.1, 2, 2, 5, 2, \quad 2]^T$ km.

Figure 4 includes the four models compared in Figure 2—YA, WLD, BB, and the combination of WLD with the new J_2 corrections—as well as three models that were not included in the discussion of the example scenario above. The first of these is the Schweighart-Sedwick model that averages the effect of J_2 on near-circular orbits into a linear, time-invariant system similar to CW. Next is the combination of the new J_2 corrections with the YA solution, neglecting the second-order Keplerian effects included in WLD. Last is a propagation based on mean relative orbit elements (ROE).[20] Whereas the other models are based on RTN coordinates, this last model is based on a linearization of the orbital element dynamics and represents the state of the art in analytical relative motion modeling. For readability, the curves in Figure 4 have been color coded according to the model assumptions (red for unperturbed eccentric orbits, green for perturbed circular orbits, purple for perturbed eccentric orbits, and blue for orbital element dynamics) and style-coded according to the order of the dynamics model (dashed for linear and dash-dot for second-order).

Several notable trends appear in Figure 4. The translational state models fit a clear hierarchical pattern based on their underlying assumptions and dynamics at low eccentricities. Those that include second-order effects are more accurate than the linear models, while the inclusion of eccentricity effects is slightly more important than the inclusion of J_2 effects. Hence, the linearized Schweighart-Sedwick model is less accurate than the unperturbed YA solution, while the inclusion of partial eccentricity and J_2 effects in Butcher-Burnett results in a more accurate model. More significantly, the second-order WLD model without J_2 corrections is substantially more accurate than the J_2-corrected YA model that neglects second-order Keplerian gravity. For substantially elliptical orbits, both eccentricity and J_2 become more important. The YA and WLD solutions are less sensitive to changes in eccentricity than Butcher-Burnett, but the addition of the new J_2 corrections to the YA model results in the most consistent performance. At eccentricities above $e = 0.5$, the relative

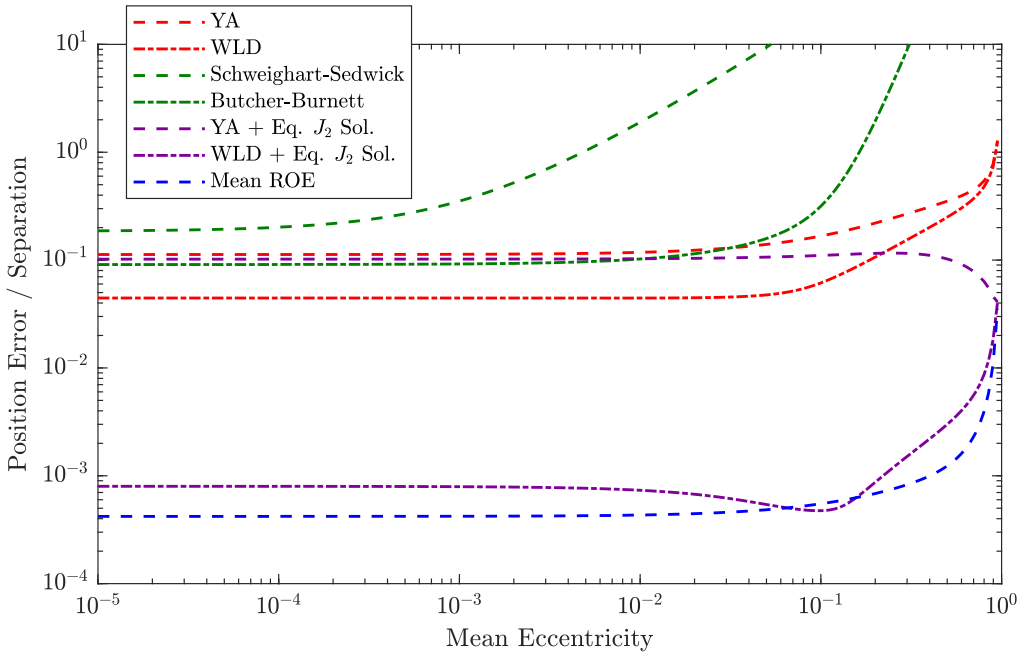

Figure 4. Average Normalized Position Error for a Range of Eccentricities with $a\mathbf{K}$ = $[0.1, 2, 2, 5, 2, \quad 2]^T$ km.

error of this model actually decreases because the separation grows with the semimajor axis, which itself increases with eccentricity due to the fixed perigee altitude.

The most remarkable feature of Figure 4 is the dramatic improvement in accuracy—nearly two orders of magnitude—that results from including both second-order Keplerian effects and the leading-order corrections for J_2 perturbation. In fact, the new solution is comparable in accuracy to the ROE model, an unprecedented achievement for models based entirely on relative position and velocity dynamics. It is important to stress that this comparison assumes perfect knowledge of the initial state of both spacecraft. The translational state models propagate the motion forward in the RTN coordinates while the ROE model converts the initial state to osculating and mean orbital elements, propagates in the mean orbital element space, then converts back to absolute coordinates and finally to relative position in the RTN frame. In practice there will be uncertainty in the initial state and the conversions between state representations add room for these errors to compound. Consequently, the new J_2-corrected model may be preferable to an orbital element model in applications dealing primarily with observable quantities such as relative position and velocity.

Effect of Inclination

Up to now it has been assumed that the chief's orbit is strictly equatorial, in line with the assumptions used to derive the J_2 corrections in the previous section. Just as orbits are never perfectly circular, even a near-equatorial orbit can be expected to have a nonzero inclination. It is therefore important to assess the sensitivity to deviations from the ideal case. The evaluation parallels that of eccentricity, beginning with the example scenario described above and varying the inclination of the chief while keeping the other state variables fixed. The resulting relative position error is shown in Figure 5, reported using the same normalization and averaging as Figure 4.

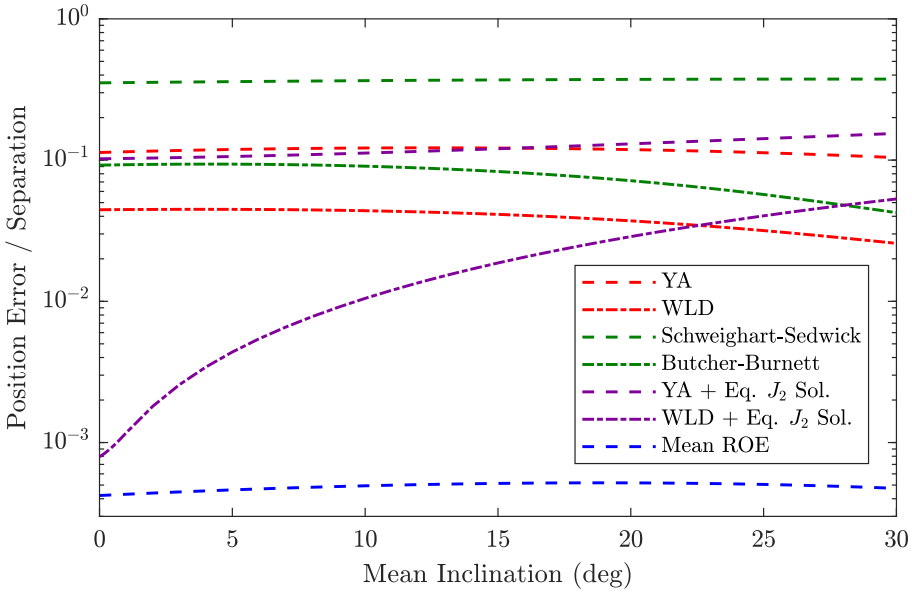

Figure 5. Average Normalized Position Error for a Range of Inclinations with $a\mathbf{K} = [0.1, 2, 2, 5, 2, \quad 2]^T$ km.

The errors shown in Figure 5 at zero inclination match those of Figure 4 at $e = 0.001$. Most of the models included in the comparison are not based on an equatorial orbit assumption and exhibit little change in accuracy across the range of inclinations considered in Figure 5. In contrast, the accuracy of the new corrections for J_2 degrades by an order of magnitude for inclinations above 10 . Despite this sensitivity, it remains the most accurate of the translational state models up to $i = 20$. The results shown in Figures 4 and 5 are intended to illustrate general patterns but only sample slices of the twelve-dimensional state space characterizing the perturbed relative motion. The exact relationships between models and how they vary with eccentricity and inclination will differ from one relative motion scenario to another.

Hyperbolic Trajectories

Although the TH equations and, by extension, the YA solution have a singularity at $e = 1$, they are valid for hyperbolic trajectories as well as for elliptical orbits. Previous work by the authors has shown that the same is true for the second-order Keplerian corrections of the WLD solution. This section explores whether the J_2 corrections developed in this work are valid for $e > 1$. Examination of the expressions appearing in the solution, both in the derivation of the previous section and in the appendix, reveals that the only terms which would be obviously problematic are the $\frac{p}{1 \quad e^2}$ terms in the definition of $\hat{e}_0$ in Equation (42). However, this definition follows the choice to use mean eccentricity from Brouwer theory in the solution evaluation. The notion of mean eccentricity is less meaningful for hyperbolic trajectories, so in this regime the osculating eccentricity at the semi-latus rectum, $f = \quad 90$, will be used as the constant reference value. With this change, $\hat{e}_0$ becomes

$$\hat{e}_0 = \left(1 + k_0 + k_0^2\right) \cos f_0 \tag{46}$$

and the problematic terms have been eliminated. Propagating this change forward, the approximation of J from Equation (45) will now be

$$J = \int \frac{d\lambda}{k^2} \quad \sqrt{\frac{\mu}{p^3}} \quad t + \frac{3}{2} J_2 \left(\frac{R_E}{p}\right)^2 \left(\sqrt{\frac{\mu}{p^3}} \frac{t}{1 \quad e^2} + \frac{\lambda \quad \lambda_0}{k^2}\right) \tag{47}$$

These are the only modifications needed to adapt the new J_2 corrections for hyperbolic trajectories.

Figure 6 extends the analysis of Figure 4 to eccentricities up to $e = 20$. The mean ROE solution and the two solutions for near-circular orbits are not valid for $e > 1$ and have been excluded from this region. For both elliptical and hyperbolic trajectories, the motion is initialized with the chief near perigee and propagated forward to $t = 10\pi\sqrt{\frac{\mu}{ja^3j}}$. The position errors shown are the average over the last 20% of the simulation. All of the solutions based on the TH equations show a large improvement in relative accuracy above $e = 1$. For $1 < e < 3$ there is little difference between the YA and WLD solutions without J_2 corrections. However, adding just the new corrections to YA gives a large improvement for $1 < e < 2$. Adding both the J_2 and second-order Keplerian corrections gives an orders-of-magnitude improvement up to $e = 10$, similar to what is observed for elliptical orbits. This demonstrates the applicability of the new relative motion model to hyperbolic trajectories and represents an important step toward interplanetary formation flying missions.

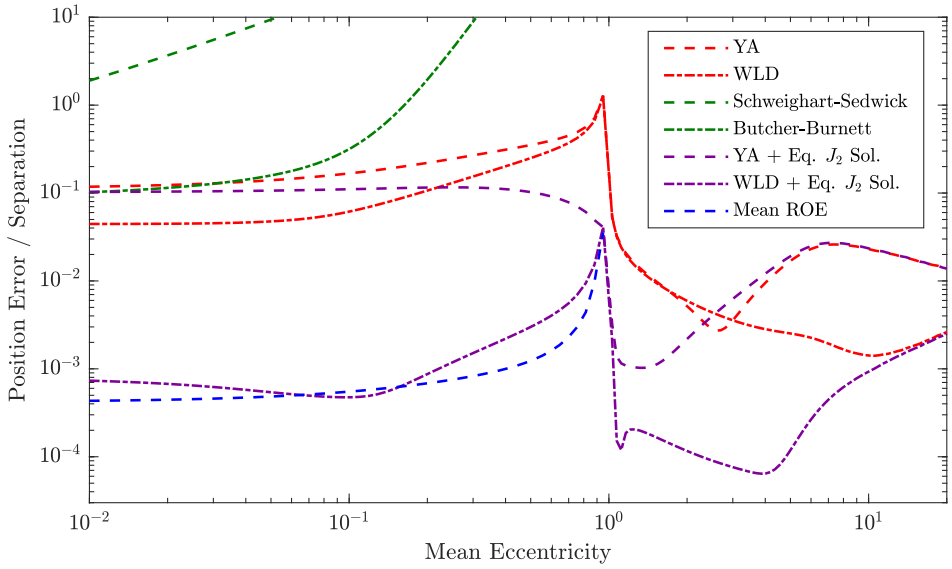

Figure 6. Average Normalized Position Error for Elliptical and Hyperbolic Trajectories with $a\mathbf{K} = [0.1, 2, 2, 5, 2, \quad 2]^T$ km.

CONCLUSION

This work includes two key contributions to spacecraft relative dynamics. The first is the explicit statement of the exact equations of relative motion in the radial-transverse-normal (RTN) coordinate frame, applicable to any perturbing force and choice of independent variable. It is common practice in the relative motion literature to introduce simplifying assumptions before applying the relevant coordinate transformations. While this is an efficient path for solving a specific problem, it obfuscates the neglected dynamics and requires a return to first principles when one wishes to

relax assumptions. The equations developed in this paper provide a rigorous starting point for any problem dealing with relative motion dynamics in the chief's RTN frame.

The second contribution is the application of the general dynamics formulation to the problem of J_2-perturbed relative motion in equatorial orbits. This demonstrates how the equations readily simplify under given assumptions while simultaneously filling a gap in the literature. Previous studies of relative motion on eccentric orbits subject to Earth oblateness perturbation used an argument of latitude formulation that was poorly defined at low-inclinations. Using true longitude as the time-like variable greatly simplifies the dynamics for equatorial orbits, allowing them to be solved analytically. The resulting solution was shown to be more accurate than previous translational state models for J_2-perturbed relative motion, which neglected or approximated the effects of eccentricity, and comparable to that of an orbital element model. Furthermore, the new solution is valid for hyperbolic trajectories as well as elliptical orbits, pushing the limits of relative motion models beyond Earth orbit.

In some ways the work presented in this paper constitutes a cohesive whole. A complete and concise form of the equations of motion were introduced and used to develop a full, analytical solution for a particular problem of interest. However, it also serves as a launching point for several future research trajectories. Earth oblateness perturbation on low-inclination orbits provided a useful demonstration of the dynamics equations and solution techniques being discussed, but the same methodology could be applied to other perturbations and regimes. In addition to environmental effects such as atmospheric drag, solar radiation pressure, and third body gravity, these might include controlled effects from continuous low-thrust propulsion. On the navigation side of the GNC domain, the accuracy and speed of the analytical models are well-suited for relative orbit determination applications using flight processors. Ultimately, these paths of research should converge, establishing a robust and efficient GNC architecture to enable future autonomous formation flying missions.

ACKNOWLEDGMENTS

This work was supported by the NASA Office of the Chief Technologist's Space Technology Research Fellowship, NASA grant number 80NSSC18K1176. The authors would also like to thank Eric Butcher and Ethan Burnett for providing the code for their higher-order solutions.

REFERENCES

[1] J. Sullivan, S. Grimberg, and S. D'Amico, "Comprehensive Survey and Assessment of Spacecraft Relative Motion Dynamics Models," *Journal of Guidance, Control, and Dynamics*, Vol. 40, No. 8, 2017, pp. 1837–1859.

[2] W. H. Clohessy and R. S. Wiltshire, "Terminal Guidance System for Satellite Rendezvous," *Journal of Guidance, Control, and Dynamics*, Vol. 27, No. 9, 1960, pp. 653–658.

[3] K. Yamanaka and F. Ankersen, "New State Transition Matrix for Relative Motion on an Arbitrary Elliptical Orbit," *Journal of Guidance, Control, and Dynamics*, Vol. 25, No. 1, 2002, pp. 60–66.

[4] J. Tschauner and P. Hempel, "Optimale Beschleunigungsprogramme fur das Rendezvous-Manover," *Astronautica Acta*, Vol. 10, No. 5-6, 1964, p. 296.

[5] H. S. London, "Second Approximation to the Solution of the Rendezvous Equations," *AIAA Journal*, Vol. 1, No. 7, 1963, pp. 1691–1693.

[6] M. L. Anthony and F. T. Sasaki, "Rendezvous Problem for Nearly Circular Orbits," *AIAA Journal*, Vol. 3, No. 7, 1965, pp. 1666–1673.

[7] M. Willis, T. A. Lovell, and S. D'Amico, "Second Order Analytical Solution for Relative Motion on Arbitrarily Eccentric Orbits," 29th AAS/AIAA Space Flight Mechanics Meeting, Ka'anapali, Maui, Hawaii, January 13-17, 2019.

[8] D. A. Vallado, *Fundamentals of Astrodynamics and Applications*. Springer, 2007.

[9] S. A. Schweighart and R. J. Sedwick, "High-Fidelity Linearized J2 Model for Satellite Formation Flight," *Journal of Guidance, Control, and Dynamics*, Vol. 25, No. 6, 2002, pp. 1073–1080.

[10] E. A. Butcher, E. Burnett, J. Wang, and T. A. Lovell, "A New, Time-Explicit J2-Perturbed Nonlinear Relative Orbit Model with Perturbation Solutions," AAS/AIAA Astrodynamics Specialist Conference, Stevenson, WA, August 20-24 2017.

[11] A. Ogundele and O. Agboola, "Power Series Solution of Nonlinear Spacecraft Relative Motion in Elliptical Orbit," AAS/AIAA Astrodynamics Specialist Conference, South Lake Tahoe, CA, August 9-13, 2020.

[12] A. Ogundele and O. Agboola, "Closed Form Solution of Nonlinear J2 Perturbed Spacecraft Formation Flying in Elliptical Orbit," AAS/AIAA Space Flight Mechanics Meeting, Charlotte, NC, February 1-4, 2021.

[13] M. Willis and S. D'Amico, "Analytical Description of Relative Position and Velocity on J2-Perturbed Eccentric Orbits," AAS/AIAA Space Flight Mechanics meeting, Charlotte, NC, February 1-4, 2021.

[14] R. G. Melton, "Time-Explicit Representation of Relative Motion Between Elliptical Orbits," *Journal of Guidance, Control, and Dynamics*, Vol. 23, No. 4, 2000, pp. 604–610.

[15] E. A. Butcher, E. Burnett, and T. A. Lovell, "Comparison of Relative Orbital Motion Perturbation Solutions in Cartesian and Spherical Coordinates," 27th AAS/AIAA Space Flight Mechanics Meeting, San Antonio, TX, February 5-9, 2017.

[16] K. T. Alfriend, S. R. Vadali, P. Gurfil, J. P. How, and L. S. Breger, *Spacecraft Formation Flying: Dynamics, control and navigation*. Elsevier, 2010.

[17] H. Schaub and J. L. Junkins, *Analytical Mechanics of Space Systems*. AIAA Education Series, 2nd ed., 2009.

[18] W. E. Boyce and R. C. DiPrima, *Elementary Differential Equations*. Wiley, 2008.

[19] M. Willis, K. T. Alfriend, and S. D'Amico, "Second-Order Solution for Relative Motion on Eccentric Orbits in Curvilinear Coordinates," AAS/AIAA Astrodynamics Specialist Conference, Portland, ME, August 11-15, 2019.

[20] A. W. Koenig, T. Guffanti, and S. D'Amico, "New State Transition Matrices for Relative Motion of Spacecraft Formations in Perturbed Orbits," AAS/AIAA Astrodynamics Specialist Conference, Long Beach, CA, September 13-16, 2016.

APPENDIX

The sections below detail the analytical expressions for the corrections to the linear relative position components that account for J_2 perturbation on equatorial orbits. In practice, these must be combined with the first-order solution of Equation (21) as shown in Equation (19). Because the corrections are derived from a linear approximation, they can be added together with similarly-derived corrections for other effects like second-order Keplerian gravity.

Radial Component

The x_2 solution is split into contributions from K_1, K_2, and K_3. Because the perturbed dynamics in Equation (43) do not depend on y_1, the solution is independent of the initial transverse separation K_4. Equation (43) also decouples the in-plane and out-of-plane motion, so K_5 and K_6 will only affect z_2. Denoting the contribution of K_i as x_{2i}, it may be written as

$$x_2 = K_1 x_{21} + K_2 x_{22} + K_3 x_{23} = \sum_{i=1}^{3} K_i x_{2i}$$

For each K_i,

$$x_{2i} = c_{x1i}\psi_1 + c_{x2i}\psi_2 + x_{2pi}$$

where ψ_1 and ψ_2 are given in Equation (28). With the assumption that the initial value of the corrections is zero, the constants c_{x1i} and c_{x2i} are computed using

$$c_{x1i} = \frac{1}{1 - e^2}\left[\psi_2'(\lambda_0)x_{2pi}(\lambda_0) - \psi_2(\lambda_0)x_{2pi}'(\lambda_0)\right]$$
$$c_{x2i} = \frac{1}{1 - e^2}\left[\psi_1(\lambda_0)x_{2pi}'(\lambda_0) - \psi_1'(\lambda_0)x_{2pi}(\lambda_0)\right]$$

The particular solution corresponding to K_1 is

$$\begin{aligned} x_{2p1} = \frac{3}{2}J_2\left(\frac{R_E}{p}\right)^2 \Bigg\{ & \frac{e_0}{2}\left[\cos\varpi_0\left(\frac{\cos\lambda}{k} - J(2k - 1)\sin\lambda\right)\right. \\ & \left. + \sin\varpi_0\left(\frac{\sin\lambda}{k} + J(2k - 1)\cos\lambda\right)\right] + \frac{1 + 2e^2}{2k}\left(1 + kk'J\right) - \frac{k}{3} + \frac{11}{6} \\ & + 2kk'J - \frac{3}{2}(\lambda - \lambda_0)\frac{k'}{k} + \frac{3}{2}J(\lambda - \lambda_0)\left(k^2 - k - k'^2\right) - \frac{3}{2}Jk^2k' \\ & \frac{1}{2}\left(1 + 2e^2 + k + k^2\right)_0\left(\frac{\cos(\lambda - \lambda_0)}{k} + J\left[k_0' - (2k - 1)\sin(\lambda - \lambda_0)\right]\right) \\ & + k_0\left(1 - \frac{1}{k} + (2k - 1)k'J\right)\Bigg\} \end{aligned}$$

which leads to

$$x_{2p1}(\lambda_0) = \frac{3}{2}J_2\left(\frac{R_E}{p}\right)^2\left\{ - \frac{e_0}{2}\frac{\cos f_0}{2k_0} + \frac{k_0}{6} + \frac{1}{3}\right\}$$
$$x_{2p1}'(\lambda_0) = \frac{3}{2}J_2\left(\frac{R_E}{p}\right)^2\left\{ - \frac{e_0}{2}\frac{\sin f_0}{k_0} + \frac{k_0'}{6} + \frac{k_0'}{2k_0}\right\}$$

The particular solution corresponding to K_2 is

$$x_{2p2} = \frac{1}{2}J_2\left(\frac{R_E}{p}\right)^2\left\{ \theta_0\left[\cos(\lambda - \varpi_0)\sin\lambda - 2\sin\varpi_0\left(1 + \frac{3}{2}kk^0J\right)\right] - 3k^2\sin\lambda \right.$$
$$+ 10k\sin\lambda + 4e_yk + \left(1 + 2e^2 - 2k_0\right)\sin\lambda - 3(\lambda - \lambda_0)(k^0\sin\lambda k\cos\lambda)$$
$$\left.\left(1 + 2e^2 + k + k^2\right)_0\left[\cos(\lambda - \lambda_0)\sin\lambda - 2\sin\lambda_0\left(1 + \frac{3}{2}kk^0J\right)\right]\right\}$$

which leads to

$$x_{2p2}(\lambda_0) = \frac{1}{2}J_2\left(\frac{R_E}{p}\right)^2\left[\theta_0(\cos f_0\sin\lambda_0 - 2\sin\varpi_0) + 4e_yk_0 + (2 + 4e^2 + 9k_0 - 2k_0^2)\sin\lambda_0\right]$$
$$x^0_{2p2}(\lambda_0) = \frac{1}{2}J_2\left(\frac{R_E}{p}\right)^2\left[\theta_0\left(\cos f_0\cos\lambda_0 - \sin f_0\sin\lambda_0 - 3\sin\varpi_0\frac{k^0_0}{k_0}\right) - 6e_x - e_xk_0\right.$$
$$\left. + (-7 + 10e^2 + 17k_0 - 7k_0^2)\cos\lambda_0 - \frac{3(1 + 2e^2)}{k_0}(\cos\lambda_0 + e_x)\right]$$

Last, the particular solution for K_3 is

$$x_{2p3} = \frac{1}{2}J_2\left(\frac{R_E}{p}\right)^2\left\{ \theta_0\left[\cos(\lambda - \varpi_0)\cos\lambda - 2\cos\varpi_0\left(1 + \frac{3}{2}kk^0J\right)\right] - 3k^2\cos\lambda \right.$$
$$+ 10k\cos\lambda + 4e_xk + (1 + 2e^2 - 2k_0)\cos\lambda - 3(\lambda - \lambda_0)(k^0\cos\lambda - k\sin\lambda)$$
$$\left.\left(1 + 2e^2 + k + k^2\right)_0\left[\cos(\lambda - \lambda_0)\cos\lambda - 2\cos\lambda_0\left(1 + \frac{3}{2}kk^0J\right)\right]\right\}$$

which leads to

$$x_{2p3}(\lambda_0) = \frac{1}{2}J_2\left(\frac{R_E}{p}\right)^2\left[\theta_0(\cos f_0\cos\lambda_0 - 2\cos\varpi_0) + 4e_xk_0 + (2 + 4e^2 + 9k_0 - 2k_0^2)\cos\lambda_0\right]$$
$$x^0_{2p3}(\lambda_0) = \frac{1}{2}J_2\left(\frac{R_E}{p}\right)^2\left[\theta_0\left(-\cos f_0\sin\lambda_0 - \sin f_0\cos\lambda_0 - 3\cos\varpi_0\frac{k^0_0}{k_0}\right) + 6e_y + e_yk_0\right.$$
$$\left.(-7 + 10e^2 + 17k_0 - 7k_0^2)\sin\lambda_0 + \frac{3(1 + 2e^2)}{k_0}(\sin\lambda_0 + e_y)\right]$$

Transverse Component

Similar to the correction in the radial direction, the transverse component has contributions from K_1, K_2, and K_3. It can be written as

$$y_2 = K_1y_{21} + K_2y_{22} + K_3y_{23} = \sum_{i=1}^{3} K_iy_{2i}$$

where

$$y_{2i} = c_{x1i}\left((1 + k)\cos\lambda - (1 + k_0)\cos\lambda_0\right) - c_{x2i}\left((1 + k)\sin\lambda - (1 + k_0)\sin\lambda_0\right)$$
$$+ 3(e_yc_{x1i} + e_xc_{x2i})k^2J - 2\int_{\lambda_0}^{\lambda} x_{2pi}d\lambda$$

The c_{x1i} and c_{x2i} are the same constants appearing in the radial corrections, and the integrals are given by

$$\begin{aligned}\int_{\lambda_0}^{\lambda} x_{2p1}\,d\lambda = \frac{3}{2}J_2\left(\frac{R_E}{p}\right)^2\Bigg[J\Bigg(-\frac{e_{y0}}{2}k\cos(\lambda - \varpi_0) + \frac{1}{2}(1+2e^2+k+k^2)k \\ \frac{1}{2}(1+2e^2+k+k^2)_0 k\cos(\lambda-\lambda_0) + \frac{k^2}{4} - \frac{3}{2}(\lambda-\lambda_0)kk' + (k_0-k)k(k-1)\Bigg) \\ + \frac{1}{6}(k_0'-k') + \frac{1}{4}(\lambda-\lambda_0)\Bigg]\end{aligned}$$

$$\begin{aligned}\int_{\lambda_0}^{\lambda} x_{2p2}\,d\lambda = \frac{1}{2}J_2\left(\frac{R_E}{p}\right)^2\Bigg[-\frac{e_{y0}}{2}(\sin(\lambda-\varpi_0)\sin\lambda - \sin(\lambda_0-\varpi_0)\sin\lambda_0) \\ + \left(k^2 - \frac{7}{2}k - \frac{13}{2} - 4e^2\right)\cos\lambda - \left(k_0^2 - \frac{7}{2}k_0 - \frac{13}{2} - 4e^2\right)\cos\lambda_0 - 2(k-k_0)(\cos\lambda - e_x) \\ + 3(\lambda-\lambda_0)\left(\frac{5}{2}e_y - k\sin\lambda\right) - \frac{1}{2}\left(1+2e^2+k+k^2\right)_0\sin(\lambda-\lambda_0)\sin\lambda \\ + \frac{3}{2}\left((1+2e^2+k+k^2)_0\sin\lambda_0 - e_{y0}\sin\varpi_0\right)k^2 J\Bigg]\end{aligned}$$

$$\begin{aligned}\int_{\lambda_0}^{\lambda} x_{2p3}\,d\lambda = \frac{1}{2}J_2\left(\frac{R_E}{p}\right)^2\Bigg[-\frac{e_{y0}}{2}(\sin(\lambda-\varpi_0)\cos\lambda - \sin(\lambda_0-\varpi_0)\cos\lambda) \\ \left(k^2 - \frac{7}{2}k - \frac{13}{2} - 4e^2\right)\sin\lambda + \left(k_0^2 - \frac{7}{2}k_0 - \frac{13}{2} - 4e^2\right)\sin\lambda_0 + 2(k-k_0)(\sin\lambda - e_y) \\ + 3(\lambda-\lambda_0)\left(\frac{5}{2}e_x - k\cos\lambda\right) - \frac{1}{2}\left(1+2e^2+k+k^2\right)_0\sin(\lambda-\lambda_0)\cos\lambda \\ + \left((1+2e^2+k+k^2)_0\cos\lambda_0 - e_{y0}\cos\varpi_0\right)\frac{3}{2}k^2 J\Bigg]\end{aligned}$$

Normal Component

Due to the decoupling of the motion for equatorial orbits, the out-of-plane motion depends only on K_5 and K_6 and is considerably simpler than the in-plane components. Expressed in terms of K_5 and K_6 it is

$$\begin{aligned}z_2 = J_2\left(\frac{R_E}{p}\right)^2\Bigg[(k-1)\left(K_5(\sin\lambda - \sin\lambda_0) + K_6(\cos\lambda - \cos\lambda_0)\right) \\ + \frac{3}{2}(\lambda-\lambda_0)\left(K_5\cos\lambda - K_6\sin\lambda\right) + 2\left(K_5 e_y + K_6 e_x\right)(\cos(\lambda-\lambda_0) - 1) \\ + \left(k_0 + \frac{1}{2}\right)\sin(\lambda-\lambda_0)\left(K_6\sin\lambda_0 - K_5\cos\lambda_0\right)\Bigg]\end{aligned}$$

Alternatively, it can be written in terms of the first order solution,

$$\begin{aligned}z_1 &= K_5\sin\lambda + K_6\cos\lambda \\ z_1' &= K_5\cos\lambda - K_6\sin\lambda\end{aligned}$$

and the initial conditions $z_0 = z_1(\lambda_0)$ and $z_0' = z_1'(\lambda_0)$, becoming

$$z_2 = J_2 \left(\frac{R_E}{p} \right)^2 \left[(k \quad 1)\,(z_1(2\cos(\lambda \quad \lambda_0) \quad 1) \quad z_0) \right.$$
$$\left. + \left(\frac{3}{2}(\lambda \quad \lambda_0) + 2k'(\cos(\lambda \quad \lambda_0) \quad 1) \right) z_1' \quad \left(k_0 + \frac{1}{2} \right) \sin(\lambda \quad \lambda_0) z_0' \right]$$